
APPROXIMATION OF CURVE-BASED SLEEVE FUNCTIONS IN HIGH DIMENSIONS

Robert BEINERT¹

¹Institut für Mathematik
Technische Universität Berlin
Straße des 17. Juni 136
10623 Berlin, Germany

14th September 2021

Correspondence

R. BEINERT: beinert@math.tu.berlin.de

Abstract. Sleeve functions are generalizations of the well-established ridge functions that play a major role in the theory of partial differential equation, medical imaging, statistics, and neural networks. Where ridge functions are non-linear, univariate functions of the distance to hyperplanes, sleeve functions are based on the squared distance to lower-dimensional manifolds. The present work is a first step to study general sleeve functions by starting with sleeve functions based on finite-length curves. To capture these curve-based sleeve functions, we propose and study a two-step method, where first the outer univariate function—the profile—is recovered, and second the underlying curve is represented by a polygonal chain. Introducing a concept of well-separation, we ensure that the proposed method always terminates and approximate the true sleeve function with a certain quality. Investigating the local geometry, we study an inexact version of our method and show its success under certain conditions.

Keywords. Sleeve functions, generalized ridge functions, adaptive learning, multivariate approximation.

AMS subject classification. 41A15, 41A30, 41A63, 65D15.

1 INTRODUCTION

The capturing or approximation of multivariate functions is nowadays one of the key elements to tackle a great number of scientific and real-world problems. A complicated function is here usually replaced by a sufficient simple function to find the numerical solution of the problem or to speed up the required numerical computations. Especially, if the domain becomes high dimensional, the approximation should rely on relatively few given function values. Unfortunately, the approximation of highly multivariate functions is hampered by the so-called curse of dimensionality [3; 16; 33]. One of the most impressive results given by NOVAK & WOŹNIAKOWSKI [33] is here the intractability of the uniform approximation of even smooth functions.

In many applications, the considered functions however possess specific low-dimensional structures that allow to overcome the curse of dimensionality. One popular approach assumes that the function of interest looks like a ridge. Mathematically, a *ridge function* $f: \mathbb{R}^d \rightarrow \mathbb{R}$ possesses the form

$$f(x) := g(Ax) \quad \text{with} \quad A \in \mathbb{R}^{\ell \times d},$$

where $\ell \ll d$. These functions are especially constant along the kernel of A . The function g is usually called the *ridge profile* whereas A is the *ridge matrix*. In the extreme case $\ell = 1$, the ridge function becomes

$$f(x) := g(\langle a, x \rangle) \quad \text{with} \quad a \in \mathbb{R}^d.$$

Although these (vector-based) ridge functions are constant along a $(d - 1)$ -dimensional subspace perpendicular to a , there are numerous applications showing their usefulness. For instance, they appear as plane waves in the theory of partial differential equations [19], play a major role in computed tomography [28], occur in statistical regression theory [8; 12], and provide the basis to analyse neural networks [5; 18; 20; 34; 35; 40]. Further, the approximation of a multivariate function by a sum of vector-based ridge functions is a topic on its own and has been studied in [1; 20; 23; 24; 29; 30; 34]. The approximation properties of matrix-based ridge functions have been considered in [27].

Due to their usefulness and approximation properties, the question arises how to learn the ridge profile and the ridge matrix/vector from certain function evaluations. A first step into this direction have been done by DEVORE, PETROVA & WOJTASZCZYK [7], who study the approximation of functions $f: \mathbb{R}^d \rightarrow \mathbb{R}$ only depending on a small set of active variables, i.e. $f(x_1, \dots, x_d) = g(x_{i_1}, \dots, x_{i_\ell})$ with $\ell \ll d$,—ridge function, whose ridge matrix consists of only unit vectors. For this, DEVORE, PETROVA & WOJTASZCZYK establish an algorithm to find the active variables and approximate the profile.

For vector-based ridge functions, a first recovery algorithm using function queries has been proposed by COHEN et al. [6], where first the ridge profile is approximated, and afterwards the ridge vector with non-negative entries is recovered using compressed sensing techniques. Overall, the algorithm performs comparable to the approximation of univariate, continuous functions with respect to the approximation rate. Another approach to tackle the recovery problem is to exploit the directional derivatives

$$\langle \nabla f(x), \phi \rangle = \dot{g}(\langle a, x \rangle) \langle a, x \rangle$$

or, more precisely, to approximate them by finite differences. Using them, FORNASIER, SCHNASS & VYBÍRAL [11] study vector-based ridge functions on the ball. Their results have then been extended to the cube by KOLLECK & VYBÍRAL [22]. In order to apply the tools from compressed sensing, the previous works assume that the ridge vector is sparse or nearly sparse. The algorithm proposed by TYAGI & CEVHER [39] uses techniques from low-rank matrix recovery—more precisely, the DANTZIG selector—to overcome the compressibility

assumption. Moreover, the recovery of vector-based ridge functions has been studied by MAYER, ULLRICH & VYBÍRAL [31], who show that the derivative of the ridge profile has to be bounded from below away from zero and that this condition is necessary in order to reduce the sampling complexity.

Essentially, a vector-based ridge function may be interpreted as a function of the distance to a $(d - 1)$ -dimensional subspace, i.e.

$$f(x) = g(\langle a, x \rangle) = g(\text{dist}(x, \mathcal{A})) \quad \text{with} \quad \mathcal{A} := \{x : x \perp a\};$$

so one possible generalization is to replace the subspace by another set. Since the level sets of the resulting f are now inflated versions of \mathcal{A} and do not look like a ridge anymore, this type of functions has been called *sleeve functions* by KEIPER [21]. More precisely, KEIPER defined a sleeve function on the basis of the squared distance, i.e.

$$f(x) := g(\text{dist}(x, \mathcal{A})^2),$$

where \mathcal{A} is a low-dimensional manifold in \mathbb{R}^d like an ℓ -dimensional subspace L with $\ell < d$. For the later case, the gradient of f becomes perpendicular to the underlying subspace L in analogy of the gradient of a vector-based ridge function. This implies that the tangent plane $\nabla f(x)^\perp$ contains L . On the basis of this observation KEIPER derived an adaptive algorithm to recover L by approximating the gradient ∇f at random points by finite differences. An alternative approach to learn L is to solve an optimization problem over the GRASSMANNIAN [21].

OUR CONTRIBUTION The focus of the present work is to study sleeve functions that are based on non-linear underlying structures. More precisely, we are interested in learning sleeve functions based on JORDAN arcs, which are injective mappings $\gamma : [0, \ell(\gamma)] \rightarrow \mathbb{R}^d$, where ℓ is the length of the arc. JORDAN arcs are thus non-self-intersecting, finite-length curves. We require that our underlying JORDAN arc is at least twice continuously differentiable—henceforth called (JORDAN) C^2 -arc or C^2 -curve. Formally, the corresponding sleeve function is defined as follows.

DEFINITION 1.1 (SLEEVE FUNCTION). Let g be in $C^2([0, \infty))$, and let $\gamma : [0, \ell(\gamma)] \rightarrow \mathbb{R}^d$ be a JORDAN C^2 -arc. The function $f : \mathbb{R}^d \rightarrow \mathbb{R}$ given by

$$f(x) := g((\text{dist}(x, \gamma))^2)$$

is called a *curve-based sleeve function*.

Our main interest is to capture the *sleeve profile* g and the *underlying curve* γ numerically from point and gradient queries, where the gradient may also be approximated by finite differences. To analyse the proposed algorithm, we require that the profile is bounded from below away from zero at the origin and that the JORDAN curve remains non-self-intersecting if it is inflated to some extent. Our central contributions are the following:

- We propose an adaptive, two-step learning algorithm to approximate the profile and to recover the underlying curve on the basis of projections that are computed from function and gradient queries. The algorithm always terminates and captures the underlying curve and profile up to given approximation errors.
- We analyse the effect of inaccurately computed projections to the proposed method recovering the underlying curve and show that the additional error can be controlled under suitable assumptions.
- We derive a uniform bound of the approximation error for the composed two steps of the proposed method.

ROADMAP After starting with some preliminaries in Section 2, we introduce the concept of well-separated JORDAN curves enforcing an extended non-self-intersecting property and an bounded curvature. The consequences regarding projection and distance to a curve are studied in Section 3. Using the well-separation, we calculate the maximal approximation error caused by replacing an arc by a polygonal chain, see Section 4. In Section 5, we derive the second step of our capturing algorithm, which recovers the underlying curve by computing projections from function and gradient queries, and study the influence of numerical errors during the projection. Capturing the sleeve profile, which builds the first step of the method, we propose an adaptive learning algorithm and bound the corresponding approximation error in Section 6. We conclude with some numerical experiments in Section 7 showing that the method can be implemented and considering some special cases.

2 PRELIMINARIES

To simplify the notation, we throughout—up to the numeric section—assume that the JORDAN arc γ is parameterized via the arclength, i.e. $\gamma : [0, \ell(\gamma)] \rightarrow \mathbb{R}^d$, where $\ell(\gamma)$ denotes the length. As a consequence the tangent vector is normalized, i.e. $\|\dot{\gamma}(t)\| = 1$ for $t \in [0, \ell(\gamma)]$, and the norm of the second derivative coincides with the (unsigned) curvature $\kappa_\gamma(t) = \|\ddot{\gamma}(t)\|$ for $t \in [0, \ell(\gamma)]$. The *end points* of γ are just $\gamma(0)$ and $\gamma(\ell(\gamma))$. We refer to the remaining points $\gamma(t)$ with $t \in (0, \ell(\gamma))$ as *inner point* of the curve.

The distance of a point x to γ is now defined by $\text{dist}(x, \gamma) := \text{dist}(x, \text{ran } \gamma)$, where ran denotes the image of γ in \mathbb{R}^d , and where $\text{dist}(x, A) := \inf_{y \in A} \|x - y\|$ for general $A \subset \mathbb{R}^d$ and the EUCLIDEAN norm. Based on the distance, the projection onto γ is defined as the set-valued map

$$\text{proj}_\gamma(x) := \{y : \|x - y\| = \text{dist}(x, \gamma)\}.$$

Because of the closedness of $\text{ran } \gamma$, the distance is always attained; so the projection is never empty. If the projection is single-valued, we may interpret $\text{proj}_\gamma(x)$ as vector or point unstated, i.e. we may write $y = \text{proj}_\gamma(x)$ with $y \in \mathbb{R}^d$. If the (single-valued) projection can only be computed up to $\epsilon > 0$, we use the notation $y \approx_\epsilon \text{proj}_\gamma(x)$, where

$y \approx_\epsilon z$ means $\|x - z\| \leq \epsilon$. Denoting the cardinality of a set by $\#[\cdot]$, we call x *ambiguous* or an *ambiguity point* if $\#[\text{proj}_\gamma(x)] > 1$ and *unambiguous* or an *unambiguity point* otherwise.

To measure the distance between two curves, we rely on the HAUSDORFF distance. More generally, the HAUSDORFF distance between two arbitrary sets $A \subset \mathbb{R}^d$ and $B \subset \mathbb{R}^d$ is defined as

$$d_H(A, B) := \max \left\{ \sup_{x \in A} \text{dist}(x, B), \sup_{y \in B} \text{dist}(y, A) \right\}.$$

For two curves γ and $\tilde{\gamma}$, we define the distance between them as the HAUSDORFF distance of their images, i.e.

$$\text{dist}(\gamma, \tilde{\gamma}) := d_H(\text{ran } \gamma, \text{ran } \tilde{\gamma}).$$

For two points $P, Q \in \mathbb{R}^d$, we denote by $\overrightarrow{PQ} = (PQ)^\rightarrow$ the vector from P to Q , i.e. $(PQ)^\rightarrow = Q - P$ where P and Q are interpreted as vectors themselves. Likewise, we define the distance and projection of a point to a curve as above. The EUCLIDEAN distance between P and Q is just given by $\text{dist}(P, Q) := \|(PQ)^\rightarrow\|$. The linear line segment between $P, Q \in \mathbb{R}^d$ is denoted by $[PQ]$. For points on a curve, i.e. $P = \gamma(t)$ and $Q = \gamma(s)$, the arc of γ between them is denoted by $\gamma_{[PQ]} := \gamma([t, s])$.

Besides the EUCLIDEAN norm $\|\cdot\|$, we use the CHEBYSHEV norm $\|\cdot\|_\infty$ for vectors and the FROBENIUS norm $\|\cdot\|_F$ for matrices. The unit vectors are denoted by e_n with $n = 1, \dots, d$, and the all-ones vector by $\mathbf{1}$. We refer to the identity matrix as I . For the ball with radius ϵ around x , we write $B_\epsilon(x)$ and, for the open ball, $\dot{B}_\epsilon(x)$. The non-negative and non-positive real numbers are denoted by \mathbb{R}_+ and \mathbb{R}_- respectively—both contain zero. The cone of a set $A \subset \mathbb{R}^d$ is defined as $\text{cone } A := \{tx : x \in A, t \geq 0\}$. Finally, we denote by $C^r(X, Y)$ the r -times continuously differentiable mappings from X to Y . If X and Y are obvious, we may write $C^r(X)$ or even C^r .

3 WELL-SEPARATION OF JORDAN CURVES

Since our approximation of the unknown curve γ will be based on projections, we have to ensure that these are well defined in a neighbourhood of γ . For this, the JORDAN curve is not allowed to intersect itself even if it is inflated to some extent. To express this assumption mathematical, we use tangential and normal cones. For the image of a C^2 -curve, the *tangential cone* [36: Def 6.1] becomes

$$T_\gamma(t) := \begin{cases} \text{cone}\{\dot{\gamma}(0+)\} & \text{if } t = 0, \\ \text{span}\{\dot{\gamma}(t)\} & \text{if } t \in (0, \ell(\gamma)), \\ \text{cone}\{-\dot{\gamma}(\ell_\gamma-)\} & \text{if } t = \ell(\gamma); \end{cases}$$

so $T_\gamma(t)$ is usually spanned by the tangent and is the ray of the left-hand or right-hand derivative at the end points. The (*regular*) *normal cone* [36: Prop 6.5] is now given by

$$N_\gamma(t) := \{v : \langle v, w \rangle \leq 0 \text{ for all } w \in T_\gamma(t)\};$$

so $N_\gamma(t)$ is usually the hyperplane orthogonal to the tangent $\dot{\gamma}(t)$ and a half-space at the end points.

DEFINITION 3.1 (WELL-SEPARATION). A JORDAN curve $\gamma: [0, \ell(\gamma)] \rightarrow \mathbb{R}^d$ is ρ -separated if

$$\mathring{B}_\rho(\gamma(t) + \rho v) \cap \text{ran } \gamma = \emptyset$$

for all $t \in [0, \ell(\gamma)]$ and $v \in N_\gamma(t)$ with $\|v\| = 1$.

Figuratively, the well-separation means that γ is not allowed to intersect with an inflated circle around the curve. Henceforth, we call the inflated circle

$$R_\gamma(t) := \bigcup_{\substack{v \perp \dot{\gamma}(t) \\ \|v\|=1}} \mathring{B}_\rho(\gamma(t) + \rho v)$$

the *normal ring* of γ at $t \in (0, \ell(\gamma))$. In three dimensions, the normal ring looks like a threaded horn torus or water wing. At the end points, the normal ring is closed with a half-ball. Up to a local neighbourhood, the points of γ are thus well-separated by a distance of 2ρ at the least. Further, the curvature of γ is bounded by $1/\rho$ since the osculating circle would then be included in the boundary of the normal ring.

The well-separation ensures the single-valueness of the projection within a certain neighbourhood of the curve.

THEOREM 3.2 (SINGLE-VALUED PROJECTION). *Let the JORDAN C^2 -arc $\gamma: [0, \ell(\gamma)] \rightarrow \mathbb{R}^d$ be ρ -separated, and let $x \in \mathbb{R}^d$ be a point with $\text{dist}(x, \gamma) < \rho$. The projection $\text{proj}_\gamma(x)$ is then single-valued and thus unique in an open neighbourhood of x .*

Proof. If $P = \gamma(t)$ is contained in $\text{proj}_\gamma(x)$, then $x - P$ has to be in the normal cone $N_\gamma(t)$, see [36: Ex 6.16]. Therefore, the ball $B_\sigma := B_\sigma(x)$ with radius $\sigma := \|x - P\| < \rho$ is contained in $B_\rho := B_\rho(P + (x-P)/\|x-P\|)$, which is the closure of a ball in the normal ring. Since the interior of B_ρ contains no points of γ , and since B_σ touches ∂B_ρ at exactly one point, the intersection $B_\sigma \cap \text{ran } \gamma$ consists only of the point P showing that the projection is single-valued. The same argumentation holds for all points in $\mathring{B}_\epsilon(x)$ with $\epsilon < \rho - \text{dist}(x, \gamma)$. \square

More general, if $x \in \mathbb{R}^d$ is no ambiguity point and does not lie on γ , we always find a small neighbourhood where the projection is single-valued too. Moreover, the set of ambiguity points is a set of measure zero. To study the set of ambiguity points, we use that the projection and distance onto and to a JORDAN C^2 -curve is differentiable for most unambiguity points. Both results can be found in [10], and we state them for our specific setting with C^2 -curves.

THEOREM 3.3 (DUDEK–HOLLY [10: THM 4.1]). *Let γ be a JORDAN C^2 -arc, and let $x \in \mathbb{R}^d$ be a point within an open neighbourhood where the projection is single-valued. If $\text{proj}_\gamma(x)$ is an inner point, then proj_γ is differentiable at x .*

The restriction to a point that is projected to an inner point is here crucial since the projection becomes undifferentiable at the end points.

Counterexample 3.4 (End Points). Consider the curve or line segment $\gamma(t) := (t, 0)^T$ with $t \in [0, 1]$. For $x := (0, 1)^T$, the derivative in direction $(1, 0)^T$ is $(1, 0)^T$ but $(0, 0)^T$ in direction $(-1, 0)^T$. Thus the projection is not differentiable at points $x := \gamma(0) + v$ with $v \perp \dot{\gamma}(0+)$ and $\text{proj}_\gamma(x) = \gamma(0)$. \circ

The distance to a curve is obviously not differentiable for points on the curve. In difference to the projection, the distance is differentiable for points projected onto the end points.

THEOREM 3.5 (DUDEK–HOLLY, [10: PROP 4.4]). *Let γ be a JORDAN C^2 -arc, and let $x \in \mathbb{R}^d$ be a point within an open neighbourhood where the projection is single-valued. If $x \notin \text{ran } \gamma$, then dist_γ is differentiable at x with*

$$\nabla_x \text{dist}(x, \gamma) = \frac{x - \text{proj}_\gamma(x)}{\|x - \text{proj}_\gamma(x)\|}.$$

Proof. For points x projected to inner points, then statement has been established in [10]. If x is in a neighbourhood projected to one end point, the statement is clear since the distance becomes the EUCLIDEAN distance to the end point. The interesting points are thus $x := \gamma(0) + v$ with $v \perp \dot{\gamma}(0+)$ and $\text{proj}_\gamma(x) = \gamma(0)$. On one side of the affine hyperplane corresponding to $\dot{\gamma}(0)$ the points are projected to an inner point and on the other side to the end point. The corresponding derivatives are

$$\nabla_y \text{dist}(y, \gamma) = \frac{y - \text{proj}_\gamma(y)}{\|y - \text{proj}_\gamma(y)\|} \quad \text{and} \quad \nabla_y \text{dist}(y, \gamma) = \frac{y - \gamma(0)}{\|y - \gamma(0)\|}.$$

For $y \rightarrow x$ in both half-spaces, the derivatives converges to the same value since the projection is continuous. \square

The ambiguity points with respect to a JORDAN C^2 -curve have a benign structure. The restriction $A_2 := \{x \in \mathbb{R}^d : \#[\text{proj}_\gamma(x)] = 2\}$ of the ambiguity set $A := \{x \in \mathbb{R}^d : \#[\text{proj}_\gamma(x)] > 1\}$ consisting of all the points with exactly two projections has LEBESGUE measure zero.

LEMMA 3.6 (AMBIGUITY POINTS). *Let γ be a finite-length JORDAN C^2 -arc. Then the subset $A_2 := \{x \in \mathbb{R}^d : \#[\text{proj}_\gamma(x)] = 2\}$ has LEBESGUE measure zero.*

Proof. Let x be an ambiguity point in A_2 with projection P_1 and P_2 . Since the distance function is continuous, we find a small open neighbourhood U_x such that $\text{dist}(y, \gamma)$ is attained by a curve point near P_1 and/or P_2 , i.e. $\text{dist}(y, \gamma) = \min\{\text{dist}(y, \gamma_1), \text{dist}(y, \gamma_2)\}$, where γ_1 and γ_2 are small arcs around P_1 and P_2 . Further U_x may be chosen small enough such that the projection to a single arc γ_1 or γ_2 is single-valued in U_x such that proj_{γ_1} and proj_{γ_2} become continuously differentiable by Theorem 3.3. The ambiguity points in U_x are the zeros of the function

$$F: U_x \rightarrow \mathbb{R} : y \mapsto \text{dist}(y, \gamma_1) - \text{dist}(y, \gamma_2).$$

Because the gradient

$$\nabla F(x) = \frac{x - P_1}{\|x - P_1\|} - \frac{x - P_2}{\|x - P_2\|}$$

is non-zero, P_1 and P_2 are distinct points, DINI's implicit function theorem [9: Thm 1B.1] states that the ambiguity set A_2 in an open neighbourhood $\tilde{U}_x \subset U_x$ around x is the realization of a continuously differentiable map $a_x: \mathbb{R}^{d-1} \rightarrow \mathbb{R}^d$ and thus a LEBESGUE zero set by SARD' theorem [37]. Since the EUCLIDEAN \mathbb{R}^d is second-countable, already countably many set U_{x_n} cover A_2 , whose union is again a LEBESGUE zero set. \square

PROPOSITION 3.7 (AMBIGUITY POINTS). *Let γ be a JORDAN C^2 -arc. Then the ambiguity set $A := \{x \in \mathbb{R}^d : \#[\text{proj}_\gamma(x)] > 1\}$ is the closure of A_2 .*

Proof. Since the distance to the curve is continuous, the points in $\overline{A_2}$ are ambiguous. To show $A \subset \overline{A_2}$, we take an ambiguity point x with $\#[\text{proj}_\gamma(x)] > 2$. In two dimensions, the set $\text{proj}_\gamma(x)$ is located on a circle. Since γ is not closed, we can either shrink the circle and move it into a gap between to projection points or, if $\text{proj}_\gamma(x)$ lie on a half-sphere, we can move the circle outwards and enlarge it, see Figure 1. In both cases, the center y of the deformed circle is contained in A_2 . By controlling the radius, the center may be arbitrary close to x . This construction generalizes to \mathbb{R}^d by changing the radius and moving the sphere containing the projection points in several steps. \square

Figuratively, higher ambiguities with $\#[\text{proj}_\gamma(x)] > 2$ occur at points, where the charts constructed by the implicit function theorem are glued together. Since A_2 is locally a hypersurface, the LEBESGUE measure of the closure remains zero. On the basis of a different argumentation, the statement has already by shown by HASTIE & STUETZLE [14; 15] for smooth curves.

THEOREM 3.8 (HASTIE-STUETZLE, [15: PROP 6]). *Let γ be a JORDAN C^2 -arc. Then the ambiguity set $A := \{x \in \mathbb{R}^d : \#[\text{proj}_\gamma(x)] > 1\}$ has LEBESGUE measure zero.*

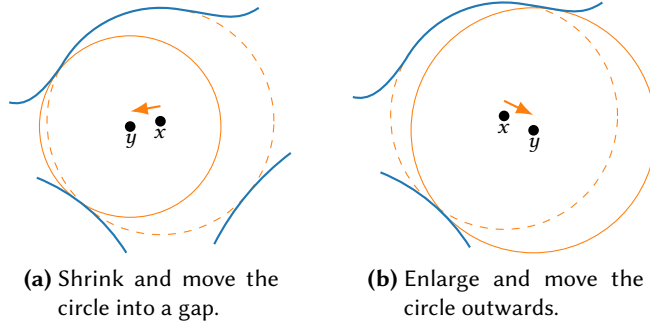


Figure 1: The projections of the ambiguity point x onto the **curve** γ lie on a **circle**. Changing the radius and moving the circle around, we find an arbitrary close point with exactly two projection.

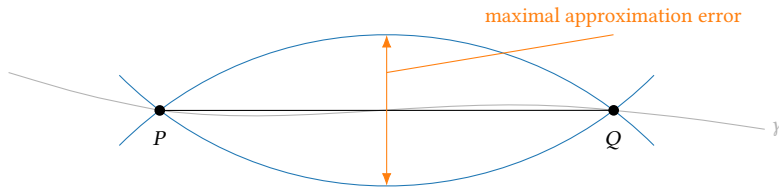


Figure 2: The two circles correspond to the **worst-case normal rings** at P that touch Q and vice versa. The **maximal approximation error** may be attained in the middle of $[PQ]$.

4 APPROXIMATION BY POLYGONAL CHAINS

If the curvature of a planar curve γ is bounded by κ_{\max} , then the approximation error between an arc $\gamma_{[PQ]}$ and the line segment $[PQ]$ is bounded by

$$\text{dist}(\gamma_{[PQ]}, [PQ]) \leq \frac{\ell^2(\gamma_{[PQ]})}{2} \kappa_{\max},$$

see [4]. Since we however have no information about the current arc $\gamma_{[PQ]}$ living in \mathbb{R}^d , we use a more geometric consideration to estimate the maximal approximation error.

THEOREM 4.1 (APPROXIMATION ERROR). *Let $\gamma: [0, \ell(\gamma)] \rightarrow \mathbb{R}^d$ be a ρ -separated JORDAN C^2 -arc, and let P and Q be distinct points on γ such that $h := \text{dist}(P, Q) < 2\rho$. The maximal approximation error is then bounded by*

$$\text{dist}(\gamma_{[PQ]}, [PQ]) \leq \rho - \sqrt{\rho^2 - \frac{h^2}{4}}.$$

Proof. We first discuss the planar setting, where the normal ring becomes the union of two open discs of radius ρ for inner points and is extended by an open half-disc of radius

2ρ at the end points. By the ρ -separation, the normal rings of $\gamma_{[PQ]}$ are not allowed to cover P or Q . To estimate the approximation error, let us consider the worst-case normal rings at P that also touch Q and vice versa, i.e. the two discs of radius ρ touching P and Q . The situation is schematically shown in Figure 2. The main observation is now that the arc $\gamma_{[PQ]}$ has to lie in the intersection of the two discs. For this, we notice two things: 1. γ cannot cross the boundary of the intersection except at P and Q since otherwise the normal ring at the crossing point would cover P or Q ; 2. γ cannot start in the intersection, leave at P , go around the intersection, and enter again at Q due to the end point condition of the ρ -separability. Since the two circular segment shown in Figure 2 are possible paths for $\gamma_{[PQ]}$, the maximal HAUSDORFF approximation error is attained in the middle of $[PQ]$. The PYTHAGOREAN theorem now yields the assertion.

Similarly in higher dimensions, $\gamma_{[PQ]}$ is contained in the intersections of all open balls of radius ρ touching P and Q . Possible arcs from P to Q with maximal HAUSDORFF approximation error are the circular segments of a two-dimensional cut through the intersection containing P and Q , which looks exactly as in the planar setting. The assertion again follows by the PYTHAGOREAN theorem. \square

If the end points P and Q of $\gamma_{[PQ]}$ are inaccurate, the error analysis may be adapted by enlarging the area that contains the true arc.

COROLLARY 4.2 (APPROXIMATION ERROR). *Let $\gamma: [0, \ell(\gamma)] \rightarrow \mathbb{R}^d$ be an ρ -separated JORDAN C^2 -arc, and let \tilde{P}, \tilde{Q} with $\text{dist}(\tilde{P}, P) \leq \epsilon$, $\text{dist}(\tilde{Q}, Q) \leq \epsilon$, and $h := \text{dist}(\tilde{P}, \tilde{Q}) < 2(\rho - \epsilon)$ be approximations of the curve points P, Q . The maximal approximation error of the arc $\gamma_{[PQ]}$ is bounded by*

$$\text{dist}(\gamma_{[PQ]}, [\tilde{P}\tilde{Q}]) \leq \rho + \epsilon - \sqrt{\rho^2 - \frac{(h+2\epsilon)^2}{4}}.$$

Proof. Extend the line $[\tilde{P}\tilde{Q}]$ by a segment of length ϵ on both ends and move the constructed circular segments in every two-dimensional cut away from the approximation line by ϵ to cover the true end points of the arc $\gamma_{[PQ]}$. \square

The above estimate only considers the distance between the curve points and the maximal curvature encoded in the well-separation. It is possible to improve the bounds using tangents at P and Q additionally. In doing so, the main improvement can be seen for the approximation of long arcs $\gamma_{[PQ]}$. To control the HAUSDORFF approximation error numerically without knowing the curve itself, the length of the line segments has to be rather small such that the angle between the tangents and the direction of the polygonal line segment is negligible.

5 RECONSTRUCTION OF THE UNDERLYING JORDAN CURVE

The identification of a curve-based sleeve function consists of two central part. One the one side, we have the approximate the unknown structure function g and, on the other

side, the underlying curve γ . Assume for this section that the differentiable structure function $g: [0, \infty] \rightarrow \mathbb{R}$ is strictly monotonically increasing with $g(0) = 0$ and $\dot{g} \gg 0$ and is known in advance. For any point $x \in \text{ran } \gamma$, the sleeve function f thus becomes zero. Otherwise, if x is unambiguous, Theorem 3.5 ensures that f is differentiable with gradient

$$\begin{aligned} \nabla f(x) &= 2\dot{g}((\text{dist}(x, \gamma))^2) \text{dist}(x, \gamma) \frac{x - \text{proj}_\gamma(x)}{\|x - \text{proj}_\gamma(x)\|} \\ &= 2\dot{g}((\text{dist}(x, \gamma))^2) (x - \text{proj}_\gamma(x)); \end{aligned}$$

so the negative gradient points directly to $\text{proj}_\gamma(x)$. Moreover, the distance to the curve is encoded in the function value $f(x)$ and may be determined by inverting the strictly monotone g . Together, this allow us to compute the projection to the unknown curve by evaluating f and ∇f .

ALGORITHM 5.1 (PROJECTION TO UNDERLYING JORDAN CURVE).

INPUT: $x \in \mathbb{R}^d$, $f: \mathbb{R}^d \rightarrow \mathbb{R}$, $g: \mathbb{R}^d \rightarrow \mathbb{R}$.

- (1) Evaluate $z := f(x)$.
- (2) Compute $t := g^{-1}(z)$.
- (3) Determine $v := \nabla f(x)$.
- (4) Set $y := x - \sqrt{t} \|v\|^{-1} v$.

OUTPUT: $y = \text{proj}_\gamma(x)$.

On the basis of this projection, we approximate the underlying curve by a polygonal chain. If $[PQ]$ is the last line segment, we consider $Q + s(PQ)^\rightarrow$, which may be seen as extension of the segment in direction of Q , and project this point back to γ by Algorithm 5.1. If the step size s is chosen appropriately, the distance of the new point to Q can be controlled from below and from above.

THEOREM 5.2 (STEP SIZE GUARANTEE). *Let $\gamma: [0, \ell(\gamma)] \rightarrow \mathbb{R}^d$ be a ρ -separated JORDAN C^2 -arc, and let P and Q be distinct points on γ such that $h := \text{dist}(P, Q) \leq \eta$ for $\eta < \rho$. Then $R := \text{proj}_\gamma(Q + s_* v)$ with $v := (PQ)^\rightarrow / \text{dist}(P, Q)$ and $s_* := (\eta^2 + 2\eta\rho) / (2\rho + 2\eta + h)$ satisfies*

$$\frac{6}{80} \eta \leq \text{dist}(R, Q) \leq \eta,$$

or, if the lower bound does not hold, R is an end point of γ .

Proof. Due to the restriction $\eta < \rho$, the parameter s_* is bounded by $3/4 \rho$; so the distance between the point $\tilde{R} := Q + s_* v$ and γ is ρ at the most, which ensures that the projection onto γ is unique, and that R is hence well defined. Next, we study the maximal possible projection distance $\delta_s := \text{dist}(R_s, \tilde{R}_s)$ with $R_s := \text{proj}_\gamma(\tilde{R}_s)$ and $\tilde{R}_s := Q + sv$ for arbitrary step sizes s . Because of the ρ -separation, the normal ring around Q is not allowed to

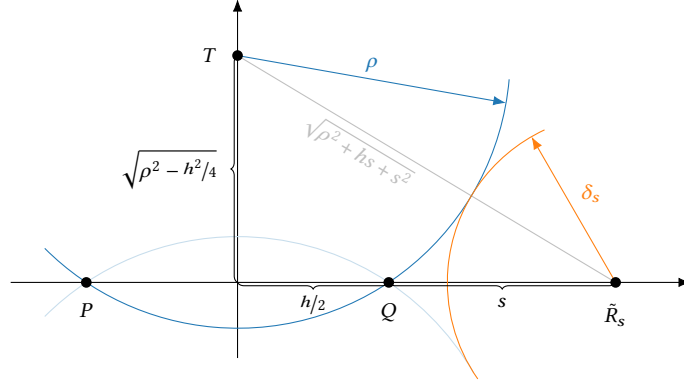


Figure 3: Calculation of the **maximal projection distance** of the point \tilde{R}_s onto γ based on the **worst-case normal rings**.

cover P ; so the path of γ after Q is limited by considering all possible normal rings. In two dimensions, the path is bounded by two discs, see Figure 3, in higher dimensions, by the union of all balls touching P and Q . If γ does not end near Q , the maximal possible projection distance is reached if $B_{\delta_s}(\tilde{R}_s)$ touches the union. The other way round, if δ_s becomes greater, then γ cannot leave the neighbourhood of Q and R_s is an end point.

If γ does not end, the maximal possible projection distance can be explicitly computed by considering a two-dimensional cut through the rotational invariant geometry as shown in Figure 3 and is given due to the PYTHAGOREAN theorem by

$$\delta_s = \sqrt{\rho^2 + hs + s^2} - \rho.$$

For a fixed s , the distance between R_s and Q is thus bounded by

$$s - \delta_s \leq \text{dist}(R_s, Q) \leq s + \delta_s.$$

The step size s_* in the assertion is the unique solution of

$$\sqrt{\rho^2 + hs + s^2} = \eta + \rho - s,$$

which ensures that the upper bound becomes exactly η .

Inserting s_* into the lower bound, we obtain

$$s_* - \delta_{s_*} = \frac{\eta^2 + 2\eta\rho}{2\rho + 2\eta + h} - \sqrt{\rho^2 + h \frac{\eta^2 + 2\eta\rho}{2\rho + 2\eta + h} + \left(\frac{\eta^2 + 2\eta\rho}{2\rho + 2\eta + h}\right)^2} + \rho.$$

Note that the lower bound is monotonically decreasing with respect to h because the path of γ is less restricted for larger h resulting in an increasing maximal projection distance δ_s ; so the lower bound is limited by

$$s_* - \delta_{s_*} \geq \frac{\eta^2 + 2\eta\rho}{2\rho + 3\eta} - \sqrt{\rho^2 + \frac{\eta^3 + 2\eta^2\rho}{2\rho + 3\eta} + \left(\frac{\eta^2 + 2\eta\rho}{2\rho + 3\eta}\right)^2} + \rho > 0.$$

Rearranging the argument of the square root, we have

$$t_1 := \rho^2 + \frac{\eta^3 + 2\eta^2\rho}{2\rho + 3\eta} + \left(\frac{\eta^2 + 2\eta\rho}{2\rho + 3\eta}\right)^2 = \frac{4\rho^4 + 17\eta^2\rho^2 + 12\eta\rho^3 + 12\eta^3\rho + 4\eta^4}{(2\rho + 3\eta)^2}.$$

Considering the square of the remaining term yield

$$t_2 := \left(\frac{\eta^2 + 2\eta\rho}{2\rho + 3\eta} + \rho\right)^2 = \frac{(\eta^2 + 5\eta\rho + 2\rho^2)^2}{(2\rho + 3\eta)^2} = \frac{4\rho^4 + 29\eta^2\rho^2 + 20\eta\rho^3 + 10\eta^3\rho + \eta^4}{(2\rho + 3\eta)^2}.$$

Applying the mean value theorem to the square root, and exploiting $t_2 > t_1$ and $\rho > \eta$, we finally obtain

$$\begin{aligned} s_* - \delta_{s_*} &= \sqrt{t_2} - \sqrt{t_1} \geq \frac{t_2 - t_1}{2\sqrt{t_2}} \\ &\geq \frac{12\eta^2\rho^2 - 3\eta^4 + 8\eta\rho^3 - 2\eta^3\rho}{(2\rho + 3\eta)^2} \frac{2\rho + 3\eta}{2(\eta^2 + 5\eta\rho + 2\rho^2)} \\ &\geq \frac{9\eta\rho^2 + 6\rho^3}{2 \cdot (5\rho) \cdot (8\rho^2)} \eta \geq \frac{6}{80} \eta. \end{aligned} \quad \square$$

The calculated optimal step size s_* depends on $h := \text{dist}(P, Q)$. Figuratively, if the last step has been small, the region where γ runs and the related uncertainty becomes smaller resulting in a greater step size and vice versa. The guaranteed minimal and maximal step size allow us to move along the unknown curve without getting stuck. If the underlying curve is well separated, we can, moreover, control the approximation error for the obtained polygonal chain.

ALGORITHM 5.3 (UNDERLYING JORDAN CURVE APPROXIMATION).

INPUT: $\rho > 0$, $E \in (0, \rho)$, $x_0 \in \mathbb{R}^d$ with $\nabla f(x_0)$ is well defined.

INITIALIZATION:

- (1) Set $\eta := \min\{\rho, 2\sqrt{\rho^2 - (\rho - E)^2}\}$.
- (2) Compute $P_0 := \text{proj}_Y(x_0)$.
- (3) For $n = 1, 2, \dots$ until $P_0 \neq P_1$ do:
 - (a) Generate $v_n \in \mathbb{R}^d$ with $\|v_n\| = \eta/2$ and $v_n \perp \text{span}\{v_1, \dots, v_{n-1}\}$.
 - (b) Compute $P_1 := \text{proj}_Y(P_0 + v_n)$. If $P_1 = P_0$, try $P_1 := \text{proj}_Y(P_0 - v_n)$.

ITERATIONS:

- (4) For $n = 1, 2, \dots$ until $P_n = P_{n-1}$ do:
 - (a) Set $s := (\eta^2 + 2\eta\rho)/(2\rho + 2\eta + h)$ with $h := \text{dist}(P_n, P_{n-1})$.
 - (b) Compute $P_{n+1} := \text{proj}_Y(P_n + sv)$ with $v := \overrightarrow{P_{n-1}P_n}/\text{dist}(P_{n-1}, P_n)$.
- (5) For $m = 0, 1, \dots$ until $P_{-m} = P_{-m+1}$ do:
 - (a) Set $s := (\eta^2 + 2\eta\rho)/(2\rho + 2\eta + h)$ with $h := \text{dist}(P_{-m}, P_{-m+1})$.
 - (b) Compute $P_{-m-1} := \text{proj}_Y(P_{-m} + sv)$ with $v := \overrightarrow{P_{-m+1}P_{-m}}/\text{dist}(P_{-m+1}, P_{-m})$.

OUTPUT: Polygonal chain $\tilde{\gamma} := \bigcup_{k=-m+1}^{n-2} [P_k P_{k+1}]$ with $\text{dist}(\tilde{\gamma}, \gamma) \leq E$.

This algorithm starts somewhere on the underlying curve and iteratively moves in both direction until the end point of the curve is reached. Due to the guaranteed length of the appended line segments, the procedure ends after finitely many steps.

THEOREM 5.4 (TERMINATION). *Let $\gamma: [0, \ell(\gamma)] \rightarrow \mathbb{R}^d$ be a ρ -separated JORDAN C^2 -arc. For any $E \in (0, \rho)$, Algorithm 5.3 yields a polygonal chain $\tilde{\gamma}$ with $\text{dist}(\tilde{\gamma}, \gamma) \leq E$ in finite time, i.e. Algorithm 5.3 terminates.*

Proof. The chosen step size $\eta := \min\{\rho, 2(\rho^2 - (\rho - E)^2)^{1/2}\}$ ensures that all projections during the algorithm are well defined and single-valued by Theorem 3.2; so Algorithm 5.3 can be executed. The maximal step size guarantee in Theorem 5.2 further yields $\text{dist}(P_k, P_{k+1}) \leq \eta$ resulting in $\text{dist}(\gamma_{[P_k P_{k+1}]}, [P_k P_{k+1}]) \leq E$ for all line segments by Theorem 4.1. Since the length of the line segments $[P_k P_{k+1}]$ is bounded from below by Theorem 5.2, and since γ has a finite length, the iterations (4) and (5) terminate as soon as the end point is reached, which happens in finitely many steps. \square

If the required projections become inexact, in the worst case, we are maybe not able to recover the underlying JORDAN curve. For this reason, we now study the caused errors and instabilities in more detail. The central idea is to adapt the calculations in the proof of Theorem 5.2, where the maximal possible projection distance of the point $\tilde{R}_s := Q + sv$ with $v := (PQ)^\perp / \text{dist}(P, Q)$ has been computed. If the projections are inexact, then we can merely determine the points P and Q in Figure 3 up to a small neighbourhood—say up to an ϵ -ball; so instead of using ρ -balls touching P and Q to guarantee the minimal and maximal step size, we consider ρ -balls intersecting $B_\epsilon(P)$ and $B_\epsilon(Q)$. To simplify the calculations, we restrict ourselves to a specific set of balls that results from the following construction, see Figure 4:

- (i) take some ρ -ball intersecting $B_\epsilon(P)$ and $B_\epsilon(Q)$, and consider the plane through P , Q , and the centre of the ball;
- (ii) denoting the intersection points of the ρ -ball with the line through $P + \epsilon 1$ and $Q - \epsilon 1$ by \tilde{P} and \tilde{Q} ;
- (iii) rotate the ball around \tilde{P} such that intersection \tilde{Q} becomes $Q - \epsilon 1$, which enlarges the maximal projection distance; and
- (iv) rotate the ball around the new \tilde{Q} and move \tilde{P} such that $\text{dist}(\tilde{P}, \tilde{Q})$ becomes $h + 2\epsilon$ with $h := \text{dist}(P, Q)$.

Without loss of generality, we have assumed that the centre is located below P and Q within the two-dimensional cut. Analogous rotations can be applied if the centre lies above P and Q . The rotation (iv) only enlarges the maximal projection distance corresponding to the original ρ -ball if ρ is large compared to h .

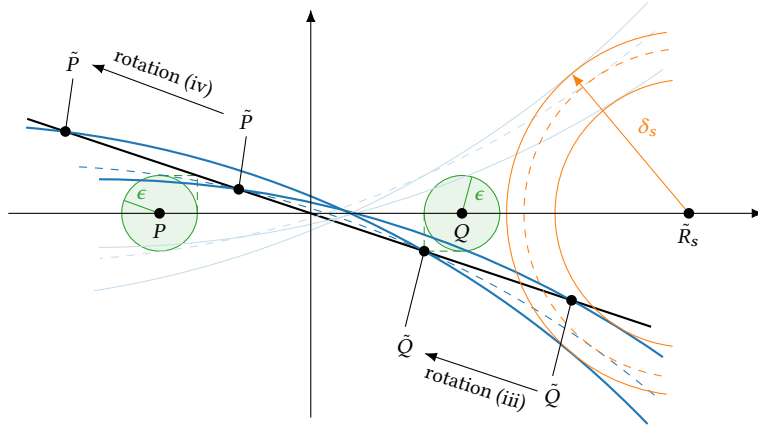


Figure 4: Rotating a **specific ball** of the normal ring intersecting the ϵ -balls around P and Q to standardize the local scenery. Both rotations (iii) and (iv) enlarge the estimation of the **maximal projection distance** for \tilde{R}_s .

LEMMA 5.5. *If $\sqrt{10}(h + 2\epsilon)/2 \leq \rho$, $s \geq \epsilon$, and $\epsilon \leq h/4$ with $h := \text{dist}(P, Q)$, then the rotation (iv) enlarges the maximal projection distance with respect to \tilde{R}_s .*

Proof. Figuratively, the maximal projection distance is enlarges as long as the circle of the maximal possible projection distance around \tilde{R}_s touches the rotated ρ -ball on the right-hand side of \tilde{Q} . More precisely, we consider the worst-case scenario where the circle of the maximal projection distance touches the ρ -ball in \tilde{Q} for $s = \epsilon$ and $\epsilon = h/4$, see Figure 5. After the rotation, the centre of the ρ -ball has to lie at the intersection of the lines f and g . Taking \tilde{Q} as origin, we may describe the lines by the functions

$$f(t) := t + \frac{\sqrt{2}}{2}(h + 2\epsilon) \quad \text{and} \quad g(t) := \frac{t}{2}.$$

A brief computation now yields

$$\rho = \left\| \left(\sqrt{2}(h + 2\epsilon), \sqrt{2}(h + 2\epsilon)/2 \right)^T \right\| = \frac{\sqrt{10}}{2}(h + 2\epsilon).$$

For greater ρ , s and smaller ϵ , the disc of possible projection of R_s touches the ρ -ball always on right-hand side of \tilde{Q} during the rotation; so the maximal projection radius is enlarged. \square

After rotation a single ρ -ball, the scenery becomes like in Figure 6. Considering the union of all rotated balls, which is rotationally symmetric around the line through P and Q , we see that every two-dimensional cut has this geometry. Instead of deriving an analysis similar to Figure 3, we estimate how far \tilde{T} in Figure 6 is away from T in Figure 3 and use the previous results.

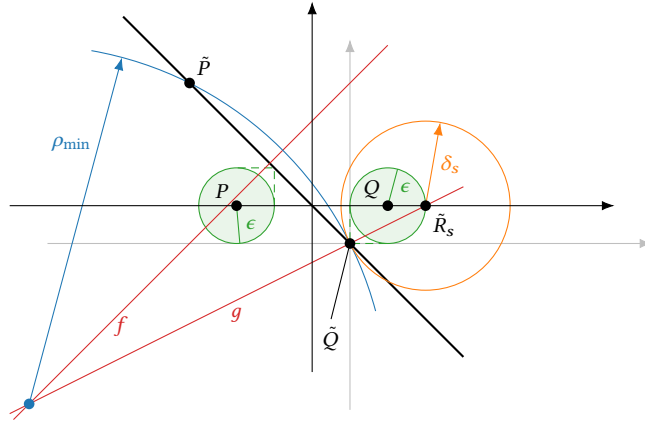


Figure 5: Worst-case scenario, where the ball with the enlarged maximal projection distance around \tilde{R}_s would touch the rotated ball in \tilde{Q} . Note that $\epsilon = h/4$, $s = \epsilon$, and $\text{dist}(\tilde{P}, \tilde{Q}) = h + 2\epsilon$. To compute the corresponding minimal radius ρ_{\min} the perpendicular bisector f of \tilde{P} and \tilde{Q} and the line g through \tilde{Q} and \tilde{R}_s is used.

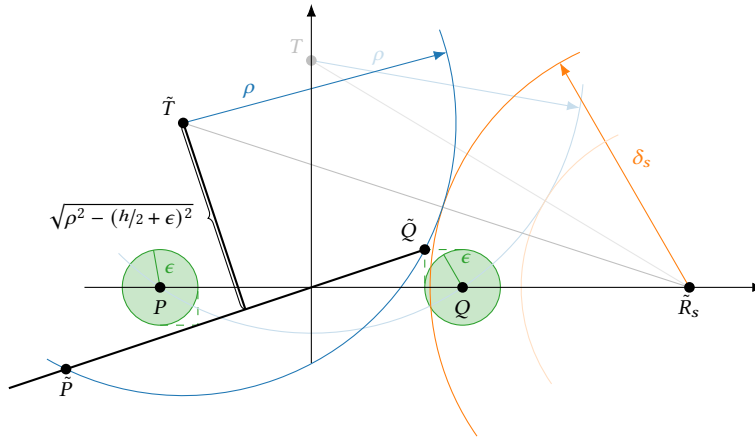


Figure 6: General situation after rotating a ρ -ball, where the centre \tilde{T} is located at the perpendicular bisector of \tilde{P} and \tilde{Q} . For comparison with Figure 3, which is indicated, we consider the mirrored ball in Figure 4. In order to estimate $\text{dist}(Q, \text{proj}_Y(\tilde{R}_s))$ from below, the radius ρ has to be much greater than in the sketch.

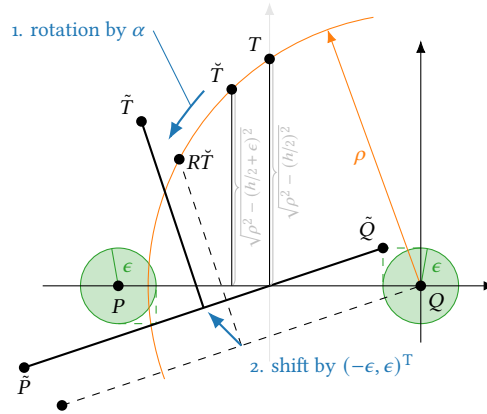


Figure 7: Calculating $\text{dist}(\tilde{T}, T)$ by noticing that \tilde{T} results from T by rotation and translation. The rotation angle α is given by $\tan \alpha = \epsilon / (h/2 - \epsilon)$.

LEMMA 5.6. *Let T be as in Figure 3 and \tilde{T} as in Figure 6. If $\sqrt{10}(h + 2\epsilon)/2 \leq \rho$ and $\epsilon \leq h/4$ with $h := \text{dist}(P, Q)$, then*

$$\text{dist}(\tilde{T}, T) \leq (\sqrt{32} \frac{\rho}{h} + 2\sqrt{2}) \epsilon.$$

Proof. Choosing Q as reference point in Figure 6, \tilde{T} is essentially a rotation followed by a shift, see Figure 7. More precisely, we have

$$\tilde{T} = R\check{T} + \begin{pmatrix} -\epsilon \\ \epsilon \end{pmatrix} \quad \text{with} \quad R = \begin{pmatrix} \cos \alpha & -\sin \alpha \\ \sin \alpha & \cos \alpha \end{pmatrix},$$

where $\tan \alpha = \epsilon/(h/2 - \epsilon)$. Preliminary, we establish the following two estimates:

1. the FROBENIUS norm distance between rotation and identity is given by

$$\|R - I\|_F^2 = 2 \left((1 - \cos \alpha)^2 + (\sin \alpha)^2 \right) = 4 (1 - \cos \alpha) = 8 (\sin \alpha/2)^2;$$

further MOLLWEIDE’s formula [32: Eq (2)] together with $\epsilon \leq h/4$ implies

$$\|R - I\|_{\text{F}}^2 \leq 8 \left(\frac{\epsilon}{(h/2 - \epsilon) + \sqrt{(h/2 - \epsilon)^2 + \epsilon^2}} \right)^2 \leq 32 \frac{\epsilon^2}{h^2};$$

2. T and \check{T} lie on the circle of radius ρ ; since $\sqrt{10}(h+2\epsilon)/2 \leq \rho$ implies $h/2+\epsilon \leq \sqrt{2}/2\rho$, the vertical distance is less than the horizontal distance; we thus infer

$$\|\check{T} - T\| \leq \sqrt{2}\epsilon.$$

Exploiting these two bounds, we finally obtain

$$\|\tilde{T} - T\| \leq \|R\tilde{T} - \tilde{T}\| + \|\tilde{T} - T\| + \|\frac{-\epsilon}{\epsilon}\|$$

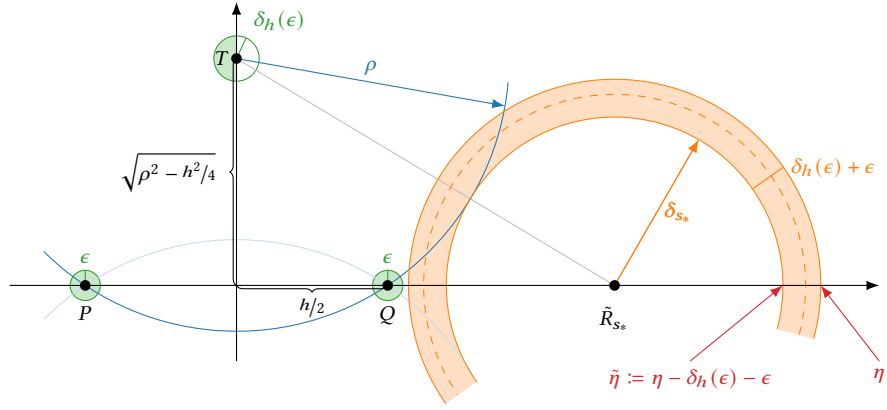


Figure 8: Incorporating the errors $\delta_h(\epsilon)$ and ϵ into the minimal and maximal step size derived in Theorem 5.2. Here s_* is lessened to guarantee $\text{dist}(Q, R) \leq \tilde{\eta}$ without uncertainties. Adding them, we have $\text{dist}(Q, R) \leq \eta$ at the most. The minimal step size is adapted similarly.

$$\begin{aligned} &\leq \|R - I\|_F \rho + \|\tilde{T} - T\| + \sqrt{2} \epsilon \\ &\leq \sqrt{32} \frac{\rho}{h} \epsilon + 2\sqrt{2} \epsilon. \end{aligned} \quad \square$$

The essential statement behind Lemma 5.6 is that the geometry exploited to establish minimal and maximal step sizes does only slightly change if the projection to obtain P and Q becomes inaccurate. Based on the projection error $\epsilon > 0$, we define

$$\delta_h := \delta_h(\epsilon) = (\sqrt{32} \frac{\rho}{h} + 2\sqrt{2}) \epsilon.$$

THEOREM 5.7 (STEP SIZE GUARANTEE). *Let $\gamma: [0, \ell(\gamma)] \rightarrow \mathbb{R}^d$ be a ρ -separated JORDAN C^2 -arc, let $\epsilon > 0$ be the maximal numerical error of proj_γ , and let P and Q be distinct points such that $\text{dist}(P, \gamma) \leq \epsilon$, $\text{dist}(Q, \gamma) \leq \epsilon$, $h := \text{dist}(P, Q) \leq \eta$ for $\sqrt{10}(h + 2\epsilon)/2 \leq \rho$, and $\epsilon \leq h/4$. If $s_* := (\tilde{\eta}^2 + 2\tilde{\eta}\rho)/(2\rho + 2\tilde{\eta} + h) \geq \epsilon$ where $\tilde{\eta} := \eta - \delta_h(\epsilon) - \epsilon$, then the numerical projection $R \approx_\epsilon \text{proj}_\gamma(Q + s_*v)$ with $v := (PQ)^\top / \text{dist}(P, Q)$ satisfies*

$$\frac{6}{80} \eta - \frac{86}{80} (\delta_h(\epsilon) + \epsilon) \leq \text{dist}(R, Q) \leq \eta,$$

or, if the lower bound is positive and does not hold, R is an approximate end point of γ .

Proof. The assumptions of the theorem ensure that the necessary rotations leading to the geometry in Figure 6 enlarge the maximal projection distance. The difference to the situation in Theorem 5.2 and Figure 3 is that T is known only approximately resulting in an uncertainty of the maximal projection distance, see Figure 8. On the basis of the step size $s_* := (\tilde{\eta}^2 + 2\tilde{\eta}\rho)/(2\rho + 2\tilde{\eta} + h)$ with $\tilde{\eta} := \eta - \delta(\epsilon) - \epsilon$, Theorem 5.2 ensures

$$\frac{6}{80} \tilde{\eta} \leq \text{dist}(R, Q) \leq \tilde{\eta}$$

for the error-free setting. Including the uncertainty $\delta_h(\epsilon)$ of the maximal projection distance and the projection error ϵ , we infer

$$\frac{6}{80} \tilde{\eta} - \delta_h - \epsilon \leq \text{dist}(R, Q) \leq \tilde{\eta} + \delta_h + \epsilon$$

yielding the assertion. \square

The lower bound of the inexact step size guarantee depends on the current h ; so the lower bound may become arbitrary small by iterating the result. Proposing an additional assumption, we may nevertheless guarantee that a slight modification of Algorithm 5.3 recovers the underlying JORDAN curve up to a certain HAUSDORFF distance even if the projection to the curve cannot be performed exactly.

THEOREM 5.8 (TERMINATION). *Let $\gamma: [0, \ell(\gamma)] \rightarrow \mathbb{R}^d$ be a ρ -separated JORDAN C^2 -arc, and let $\epsilon \in [0, \rho/4]$ be the maximal numerical error of proj_γ . Adapting Algorithm 5.3 by choosing*

$$\eta := 2 \min\{10^{-1/2} \rho, 2\sqrt{\rho^2 - (\rho + \epsilon - E)^2}\} - 2\epsilon \quad \text{and} \quad s := s_h := \frac{\tilde{\eta}_h^2 + 2\tilde{\eta}_h \rho}{2\rho + 2\tilde{\eta}_h + h}$$

with $E \in (\epsilon, \rho)$ and $\tilde{\eta}_h := \eta - \delta_h(\epsilon) - \epsilon$ yields a polygonal chain $\tilde{\gamma}$ with $\text{dist}(\tilde{\gamma}, \gamma) \leq E$ in finite time, i.e. Algorithm 5.3 terminates, if $\frac{6}{80} \eta \leq \text{dist}(P_0, P_1) \leq \eta$ and

$$\frac{6}{80} \eta - \frac{86}{80} (2\sqrt{2} + 1) \epsilon \geq \left(\frac{86}{20} \sqrt{32} \rho \epsilon\right)^{1/2}.$$

Proof. The statement may be established analogously to Theorem 5.4 as long as the guaranteed minimal step size

$$\lambda(h) := \frac{6}{80} \eta - \frac{86}{80} (\delta_h(\epsilon) + \epsilon) = \frac{6}{80} \tilde{\eta}_h - \delta_h(\epsilon) - \epsilon$$

in Theorem 5.7 does not vanish or becomes negative. First notice that $\delta_h(\epsilon)$ is inversely depending on h such that $\lambda(h)$ and $\tilde{\eta}_h$ become monotonically increasing with respect to h . Let us now assume that there exists an \tilde{h} such that

$$4\epsilon \leq \tilde{h} \leq \lambda(\tilde{h}) \leq \frac{6}{80} \tilde{\eta}_{\tilde{h}}.$$

For any $h \in [\tilde{h}, \eta]$, the step size s_h is bounded from below by

$$s_h \geq \frac{2}{5} \tilde{\eta}_h \geq \frac{6}{80} \tilde{\eta}_{\tilde{h}} \geq 4\epsilon \geq \epsilon.$$

We further have $\epsilon \leq \tilde{h}/4 \leq h/4$ and $\sqrt{10}(h + 2\epsilon)/2 \leq \rho$ due to the choice of η ; so for each $h \in [\tilde{h}, \eta]$ the requirements of Theorem 5.7 are satisfied. Since $h_1 := \text{dist}(P_0, P_1)$ is contained in $[\tilde{h}, \eta]$, Theorem 5.7 yields

$$\eta \geq \text{dist}(P_1, P_2) \geq \lambda(h_1) \geq \lambda(\tilde{h}) \geq \tilde{h}$$

and, iteratively, $\text{dist}(P_k, P_{k+1}) \in [\tilde{h}, \eta]$. For $\tilde{h} > 0$, we thus obtain the assertion.

It remains to ensure the existence of $\tilde{h} > 0$. A rearrangement of the inequality

$$\tilde{h} \leq \lambda(\tilde{h}) = \frac{6}{86} \eta - \frac{86}{80} \left(\sqrt{32} \frac{\rho}{\tilde{h}} + 2\sqrt{2} + 1 \right) \epsilon.$$

yields the quadratic inequality

$$\tilde{h}^2 + \left(\frac{86}{80} (2\sqrt{2} + 1) \epsilon - \frac{6}{80} \eta \right) \tilde{h} + \frac{86}{80} \sqrt{32} \rho \epsilon \leq 0.$$

Due to the assumptions of the theorem, we know that the discriminant

$$\Delta := \left(\frac{86}{80} (2\sqrt{2} + 1) \epsilon - \frac{6}{80} \eta \right)^2 - \frac{86}{20} \sqrt{32} \rho \epsilon$$

is non-negative, and that the centre of the non-empty solution interval satisfies

$$\tilde{h} := \frac{1}{2} \left(\frac{6}{80} \eta - \frac{86}{80} (2\sqrt{2} + 1) \epsilon \right) \geq \left(\frac{86}{20} \sqrt{32} \right)^{1/2} \epsilon \geq 4\epsilon,$$

where we exploit $\rho \geq 4\epsilon$ and again the last assumption. The existence of an appropriate $\tilde{h} > 0$ is thus guaranteed. \square

Remark 5.9. Due to the assumptions, the maximal step size η is always positive. If ϵ becomes small, then the additional assumption in Theorem 5.7 are always satisfiable. The other way round, for a given E and ρ , the theorem enable us to calculate an upper bound for the maximal projection error ϵ that guarantees the success of Algorithm 5.3 by solving a simple quadratic equation. \circ

6 IDENTIFICATION OF SLEEVE FUNCTIONS

Besides the underlying JORDAN curve, the structure function g has to be approximated too. Having a non-curve point x and its projection $y := \text{proj}_\gamma(x)$, we have immediate access to g via

$$g(t^2) = g\left(\text{dist}\left(y + t \frac{x-y}{\|x-y\|}, \gamma\right)^2\right) = f\left(y + t \frac{x-y}{\|x-y\|}\right)$$

for $t \geq 0$ until an ambiguity point is hit. Since γ is a finite-length JORDAN arc, we henceforth assume $\text{ran } \gamma \subset B_{1/2}$ for simplicity. Other domains may be considered analogously. Restricting our interest to an approximation of f on $B_{1/2}$, we only have to determine g on the interval $[0, 1]$. We have here two possibilities: either g is approximated directly or $t \mapsto g_2(t) := g(t^2)$ is approximated. We choose the second approach because g_2 immediately represent the slopes of the sleeve function.

For simplicity, we approximate g_2 by a linear spline with equispaced knots. Beneficially, this simplifies the inversion in Algorithm 5.1, where we can take $g_2^{-1}(z)$ instead of the step size \sqrt{t} . The approximation of g_2 with step size $\sigma > 0$ may be incorporated into Algorithm 5.3 for a ρ -separated JORDAN curve in the following manner: 1. From the start

point x_0 , the structure function g_2 is sampled equispaced in direction $\nabla f(x_0)$ until the curve or an ambiguity point is hit. 2. This especially gives an approximation of g_2 on $[0, \rho]$ such that Algorithm 5.3 can be performed. 3. Determine the point $x = \gamma(t)$ with the largest norm. Note that $x \perp \dot{\gamma}(t)$, that $\text{proj}_\gamma((1+s)x) = x$ for $s \geq 0$, and that the ray $\{(1+s)x : s \geq 0\}$ cannot contain any ambiguity point; so the approximation of g_2 may be extended onto $[0, 1]$ by sampling in this direction.

ALGORITHM 6.1 (SLEEVE FUNCTION APPROXIMATION).

INPUT: $\rho, \sigma > 0$, $\epsilon \in [0, \rho/4]$, $E \in (\epsilon, \rho)$, $x_0 \in \mathbb{R}^d$ where $\nabla f(x_0)$ is well defined.

INITIAL APPROXIMATION OF g_2 :

- (1) Compute $v := \nabla f(x_0) / \|\nabla f(x_0)\|$.
- (2) Collect $f_k := f(x_0 - k\sigma v)$ for $k = 0, 1, \dots$ until $f_k - f_{k-1} > 0$.
- (3) Collect $f_{-\ell} := f(x_0 + \ell\sigma v)$ for $\ell = 1, 2, \dots$ until $\sigma(k + \ell - 1) \geq \rho$.
- (4) Use $(f_j)_{j=-\ell+1}^{k-1}$ to approximate g_2 on $[0, \sigma(k + \ell - 1)]$ by a linear spline \tilde{g}_2 .

UNDERLYING JORDAN CURVE:

- (5) Apply Algorithm 5.3 modified as in Theorem 5.8 to obtain $\tilde{\gamma} := \bigcup_{j=-m+1}^{n-2} P_j P_{j+1}$.

FINAL APPROXIMATION OF g_2 :

- (6) Determine $x := \arg\max_{\{P_j: j=-m+1, \dots, n-1\}} \|P_j\|$.
- (7) Improve x by setting $y := (1 + \rho/\|x\|)x$ and $x := \text{proj}_\gamma(y)$.
- (8) Compute $v := (y - x) / \|y - x\|$.
- (9) Collect $f_r := f(x + r\sigma v)$ for $r = k + \ell, k + \ell + 1, \dots$ until $\sigma r \geq 1$.
- (10) Use these to extend the linear spline \tilde{g}_2 to approximate g_2 on $[0, 1]$.

OUTPUT: Polygonal chain $\tilde{\gamma}$, linear spline \tilde{g}_2 approximating f .

Remark 6.2. Note that the collected samples gives only rough informations about the root of $f(x_0 - tv)$, which is located somewhere around $\sigma(k-1)$. To improve the approximation of g_2 in (4), which is crucial to compute proj_γ by Algorithm 5.1, we therefore apply the NEWTON-RAPHSON method. During the numerical experiments, we usually require only a few iteration to find the root with sufficient accuracy. \circ

Due to the approximation of g_2 , the projection computed by Algorithm 5.1 becomes inexact since the true step size $g_2^{-1}(z)$ is not available. Depending on the local derivative of g_2 the approximation error is here amplified or reduced; therefore, we again assume that the projection error is again bounded by an appropriate $\epsilon > 0$. If the first and second derivative of the true structure function g are bounded, and if the step size σ is chosen appropriately, then the total approximation error for the sleeve function f may be controlled.

THEOREM 6.3 (APPROXIMATION ERROR). *Let $\gamma: [0, \ell(\gamma)] \rightarrow B_{1/2} \subset \mathbb{R}^d$ be a ρ -separated JORDAN C^2 -arc, and let $g \in C^2([0, 1], \mathbb{R}_+)$ be strictly monotonically increasing*

with

$$M_1 := \sup_{t \in [0,1]} 2|t \dot{g}(t^2)| < \infty \quad \text{and} \quad M_2 := \sup_{t \in [0,1]} |\dot{g}(t^2) + 2t^2 \ddot{g}(t^2)| < \infty.$$

If the projection error in Algorithm 5.1 is bounded by $\epsilon > 0$, and if the requirements of Theorem 5.8 are satisfied, then Algorithm 6.1 with E and σ approximates $f = g_2 \circ \text{dist}(\cdot, \gamma)$ by $\tilde{f} = \tilde{g}_2 \circ \text{dist}(\cdot, \tilde{\gamma})$ satisfying

$$\sup_{x \in B_{1/2}} |f(x) - \tilde{f}(x)| \leq M_1 E + \frac{M_2}{8} \sigma^2.$$

Proof. The first derivatives of $t \mapsto g_2(t) := g(t^2)$ are just

$$\dot{g}_2(t) = 2t \dot{g}(t^2) \quad \text{and} \quad \ddot{g}_2(t) = 2\dot{g}(t^2) + 4t^2 \ddot{g}(t^2).$$

Exploiting Theorem 5.8, the mean value theorem, and the well-established approximation error for linear splines $\|g_2 - \tilde{g}_2\|_\infty \leq \sigma^2 \|\ddot{g}_2\|_\infty / 8$, see for instance [13: Ch 6, §5.1], we have

$$\begin{aligned} |f(x) - \tilde{f}(x)| &= |g_2(\text{dist}(x, \gamma)) - \tilde{g}_2(\text{dist}(x, \tilde{\gamma}))| \\ &\leq |g_2(\text{dist}(x, \gamma)) - g_2(\text{dist}(x, \tilde{\gamma}))| + |g_2(\text{dist}(x, \tilde{\gamma})) - \tilde{g}_2(\text{dist}(x, \tilde{\gamma}))| \\ &\leq M_1 E + \frac{M_2}{8} \sigma^2. \end{aligned} \quad \square$$

7 NUMERICAL EXAMPLES

Besides the theoretical guarantees for the approximation of curve-based sleeve functions by polygonal chains and linear splines, we next present several examples to show that the established concepts may be carried out numerically. All algorithms and experiments have been implemented in Julia¹.

Oddly enough, the main obstacle is here the numerical evaluation of the true sleeve function $f(x) := g(\text{dist}(x, \gamma)^2)$ and its derivatives—even if the profile g and the underlying JORDAN curve γ are known analytically—since all computations require the projection onto γ . The projection may be computed by minimizing the function

$$\begin{aligned} F(t) &:= \|x - \gamma(t)\|^2 \\ \dot{F}(t) &= -2 \langle x - \gamma(t), \dot{\gamma}(t) \rangle \\ \ddot{F}(t) &= 2 \|\dot{\gamma}(t)\|^2 - 2 \langle x - \gamma(t), \ddot{\gamma}(t) \rangle \end{aligned}$$

over the interval $[0, \ell(\gamma)]$. For this purpose, we use the well-known NEWTON–RAPHSO method, i.e. $t_{k+1} := t_k - \dot{F}(t_k)/\ddot{F}(t_k)$, where F is sampled equispaced to find an appropriate starting value t_0 , and where the end points are considered separately. In general, the

¹The Julia Programming Language – Version 1.5.0 (<https://docs.julialang.org>)

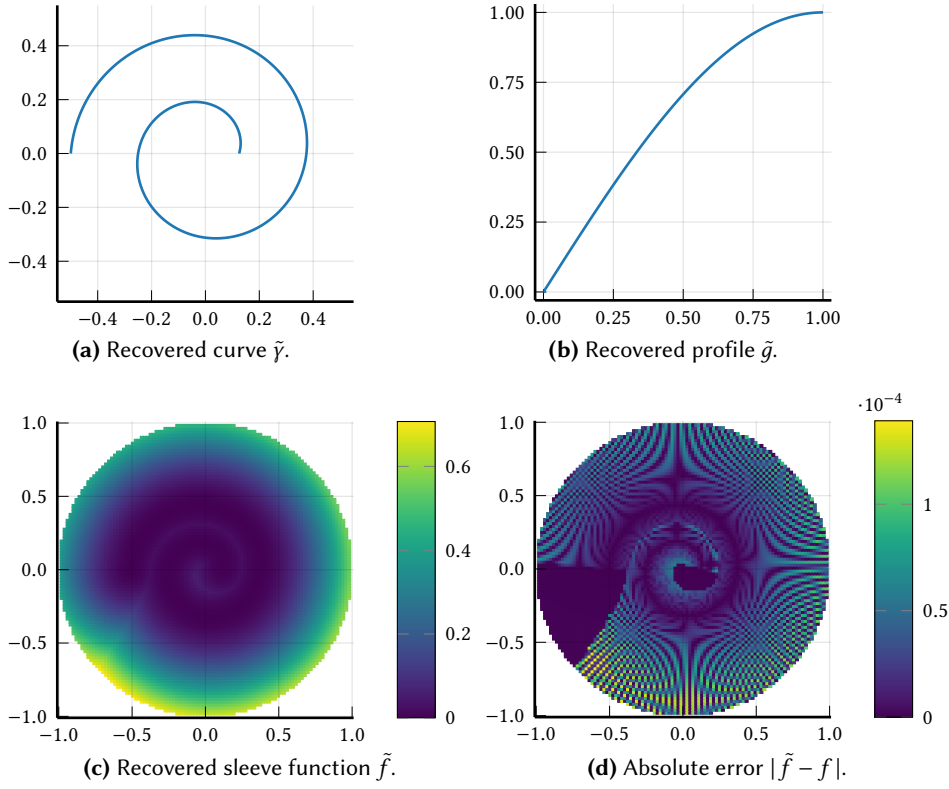


Figure 9: Sleeve function based on the ARCHIMEDEAN spiral and a sine profile. The plots only show the recovered functions since they visually coincide with the true function.

projection of a point onto a parametric curve is a non-trivial problem by itself, see for instance [17; 25; 26; 38] and references therein. In contrast, the projection to the polygonal chain γ is straightforward—project to each line segment and take the global minimizer.

ARCHIMEDEAN SPIRAL The first considered sleeve function is based on the curve

$$\gamma: [0, 1] \rightarrow \mathbb{R}^2 : t \mapsto \left(\frac{1}{8} + \frac{3t}{8}\right) \begin{pmatrix} \cos 3\pi t \\ \sin 3\pi t \end{pmatrix},$$

which is a piece of an ARCHIMEDEAN spiral, and on the profile function

$$g: [0, 1] \rightarrow [0, 1] : t \mapsto \sin(\pi/2 t).$$

The spiral is an $1/8$ -separated C^∞ -curve. Since the maximal projection error is unknown, we perform Algorithm 6.1 with $\epsilon := 0$, i.e. we assume that the error caused by the approximation of the true profile is negligible. For the remaining parameters, we choose

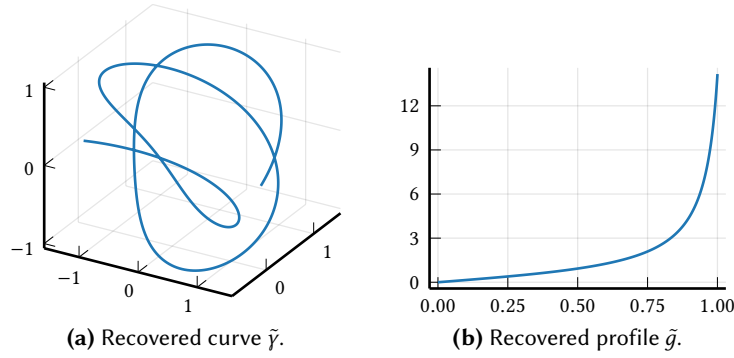


Figure 10: Sleeve function based on a space curve and a tangent profile. The plots only show the recovered functions since they visually coincide with the true function.

$E := 10^{-3}$ and $\sigma := 10^{-4}$. The result of the implemented methods is shown in Figure 9. Notice that the absolute approximation error on $B_{1/2}$ is much smaller than E , which bounds the error caused by the polygonal chain approximation of the ARCHIMEDEAN spiral. The error bound in Theorem 6.3 is here too pessimistic.

THREE-DIMENSIONAL CURVE Next, we consider the underlying curve

$$\gamma: [0, 1] \rightarrow \mathbb{R}^3 : t \mapsto \begin{pmatrix} (1 + 1/2 \cos 4\pi t) \cos 5\pi t \\ (1 + 1/2 \cos 4\pi t) \sin 5\pi t \\ \sin 4\pi t \end{pmatrix}$$

together with the profile

$$g: [0, 1] \mapsto \mathbb{R}_+ : t \mapsto \tan(3/2 t).$$

The results of Algorithm 6.1 with $\epsilon := 0$, $E := 10^{-2}$, and $\sigma := 10^{-4}$ are shown in Figure 10. Both—profile and curve—are well estimated. Since the established theoretical approximation errors are completely independent of the current dimension, we expect similar results for the two one-dimensional approximation tasks in higher dimensions.

FINITE DIFFERENCES In the last two simulations, we consider the sleeve function with respect to the $1/2$ -separated half-ellipse

$$\gamma: [0, 1] \rightarrow \mathbb{R}^2 : t \mapsto \begin{pmatrix} \cos \pi t \\ 1/2 \sin \pi t \end{pmatrix}.$$

Up to now, we have assumed that we have access to the function values and derivatives of the true sleeve function f . If the derivatives are not available, numerical differentiation

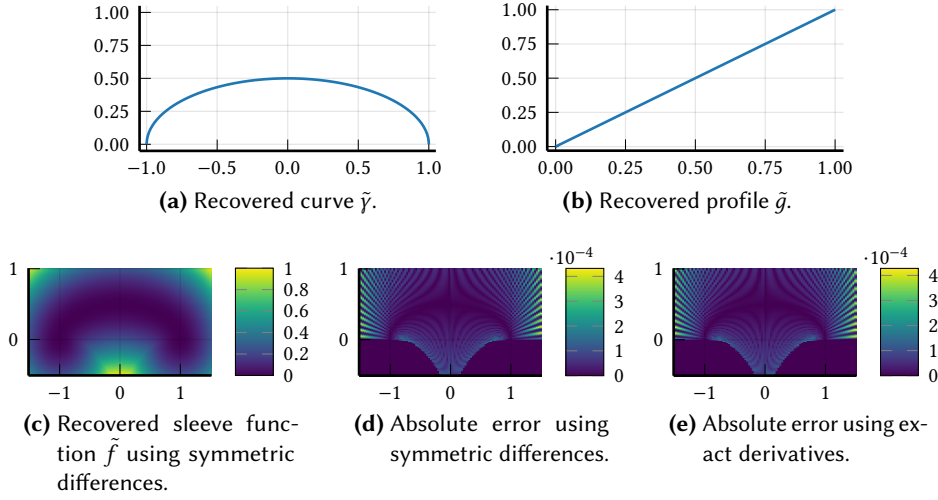


Figure 11: Sleeve function based on a half-ellipse and an identity profile. Note that the approximated profile g_2 is nevertheless non-linear. The required derivatives are approximated by symmetric difference quotients. The additional error is here marginal compared to the approximation using exact derivatives.

may be used instead. In this numerical example, we approximate the required derivatives using the symmetric difference quotient

$$[\nabla f(x)]_n \approx \frac{f(x + \tau e_n) - f(x - \tau e_n)}{2\tau}$$

for $n = 1, \dots, d$, where e_n denotes the n th unit vector. Letting the profile g be the identity, which nevertheless results in a locally non-linear sleeve function, and applying Algorithm 6.1 with the parameter set $\epsilon := 0$, $E := 10^{-3}$, $\sigma := 10^{-4}$, and $\tau := 10^{-8}$, we obtain the results in Figure 11. The additional error caused by the finite differences is here negligible.

VANISHING PROFILE In the last example, we consider again the half-ellipse but here together with the profile function $g : t \mapsto t^2$. Differently from above, the derivative \dot{g} is here not bounded away from zero on $[0, \rho]$; so the required (again exact) derivative ∇f may nearly vanish for small step sizes s . The results of the approximation with $\epsilon := 0$, $E := 10^{-2}$, and $\sigma := 10^{-4}$ is shown in Figure 12. Notice that the approximation of the underlying curve is much worse compared with the previous example. If E becomes smaller, the polygonal chain starts to oscillate around the true curve. The projection error caused by the loss of significance in Algorithm 5.1 becomes clearly visible. From a numerical point, it is crucial that \dot{g} is bounded from below away from zero although this bound does not occur in the derived approximation guarantees.

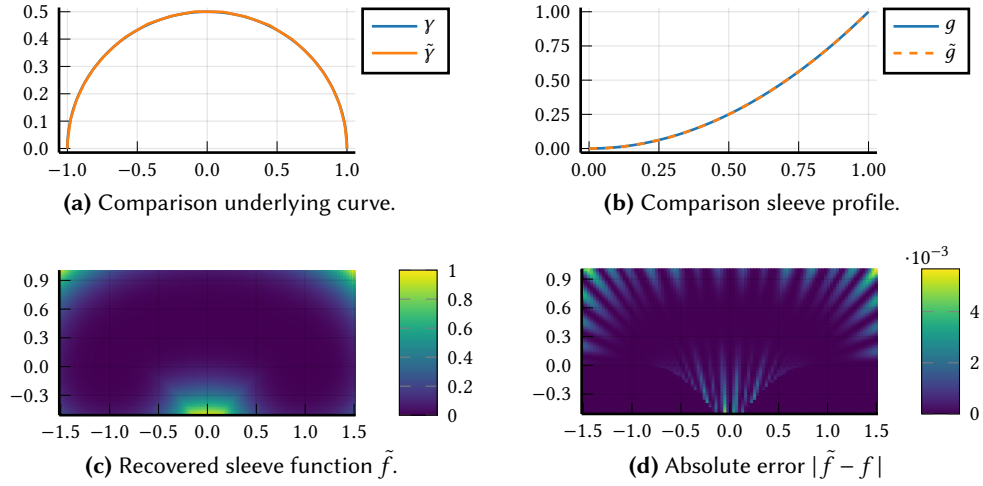


Figure 12: Sleeve function based on a half-ellipse and quadratic profile with vanishing derivative. The loss of significance during the projection with Algorithm 5.1 onto the unknown curve becomes visible—especially in the absolute error.

8 CONCLUSION

In order to capture a highly multivariate, curve-based sleeve function, we propose an two-step method that reduces the recovery problem to two one-dimensional approximation tasks. The number of samples required for the sleeve profile conforms to the one-dimensional approximation theory. The samples needed to find the underlying curve mainly depend on its length and the well-separation. The capturing of the underlying curve, which was the main interest of the present work, progresses hand over hand along the curve. Studying the geometry, we guarantee a minimal and maximal step size, which ensures that the algorithm cannot get stuck on the one hand and that the wanted quality is achieved. The derived error bounds for the two proposed one-dimensional approximations tasks are completely independence of the actual dimension. In the moment, the algorithm is based on linear approximations. If the point queries are corrupted by noise, these could be replaced by higher-order methods to improve the performance. The same applies to the required gradients, which have been partly estimated by symmetric differences during the numerical experiments. For greater uncertainties in the function evaluations, these could be replaced by higher-order differences or other techniques like extrapolation may be used. Finally, we exclusively consider curve-based sleeve functions, so it is interesting to generalize the proposed method to manifolds—either by approximating the manifold by a suitable mesh or by some geometric multi-resolution analysis [2]. The presents results are a first step to study general sleeve functions, and we believe that many results—especially the minimal/maximal step sizes—can be generalized

to manifold-based sleeve functions.

ACKNOWLEDGMENT The author is especially grateful to Sandra KEIPER, the author of [21], for many fruitful discussions and for drawing my attention to the topic of generalized ridge and sleeve functions.

REFERENCES

- [1] ALIEV, R. A., ASGAROVA, A. A., and ISMAILOV, V. E., ‘A note on continuous sums of ridge functions’, *J. Approx. Theory*, 237 (2019), 210–21. doi: 10 . 1016 / j . jat . 2018 . 09 . 006.
- [2] ALLARD, W. K., CHEN, G., and MAGGIONI, M., ‘Multi-scale geometric methods for data sets II: Geometric multi-resolution analysis’, *Appl. Comput. Harmon. Anal.* 32/3 (2012), 435–62. doi: 10 . 1016 / j . acha . 2011 . 08 . 001.
- [3] BELLMAN, R., *Adaptive control processes: A guided tour* (Princeton, N.J.: Princeton University Press, 1961).
- [4] BINEV, P. et al., ‘Adaptive approximation of curves’, Preprint Series of the Interdisciplinary Mathematics Institute, University of South Carolina – <http://imi.cas.sc.edu/papers/86/>, 2004.
- [5] CANDÈS, E. J., ‘Harmonic analysis of neural networks’, *Appl. Comput. Harmon. Anal.* 6/2 (1999), 197–218. doi: 10 . 1006 / acha . 1998 . 0248.
- [6] COHEN, A. et al., ‘Capturing ridge functions in high dimensions from point queries’, *Constr. Approx.* 35/2 (2012), 225–43. doi: 10 . 1007 / s00365 - 011 - 9147 - 6.
- [7] DEVORE, R., PETROVA, G., and WOJTASZCZYK, P., ‘Approximation of functions of few variables in high dimensions’, *Constr. Approx.* 33/1 (2011), 125–43. doi: 10 . 1007 / s00365 - 010 - 9105 - 8.
- [8] DONOHO, D. L. and JOHNSTONE, I. M., ‘Projection-based approximation and a duality with kernel methods’, *Ann. Statist.* 17/1 (1989), 58–106. doi: 10 . 1214 / aos / 1176347004.
- [9] DONTCHEV, A. L. and ROCKAFELLAR, R. T., *Implicit functions and solution mappings* (Springer Monographs in Mathematics; Dordrecht: Springer, 2009). doi: 10 . 1007 / 978 - 0 - 387 - 87821 - 8.
- [10] DUDEK, E. and HOLLY, K., ‘Nonlinear orthogonal projection’, *Ann. Polon. Math.* 59/1 (1994), 1–31. doi: 10 . 4064 / ap - 59 - 1 - 1 - 31.
- [11] FORNASIER, M., SCHNASS, K., and VYBIRAL, J., ‘Learning functions of few arbitrary linear parameters in high dimensions’, *Found. Comput. Math.* 12/2 (2012), 229–62. doi: 10 . 1007 / s10208 - 012 - 9115 - y.
- [12] FRIEDMAN, J. H. and STUETZLE, W., ‘Projection Pursuit Regression’, *J. Amer. Statist. Assoc.* 76/376 (1981), 817–23. doi: 10 . 2307 / 2287576.
- [13] HÄMMERLIN, G. and HOFFMANN, K.-H., *Numerical mathematics* (Undergraduate Texts in Mathematics; New York: Springer, 1991). doi: 10 . 1007 / 978 - 1 - 4612 - 4442 - 4.
- [14] HASTIE, T., *Principal Curves and Surfaces*, tech. rep. 11 (AD-A148 833) (Stanford: Laboratory for Computational Statistics, Department of Statistics and Computational Group, Stanford Linear Accelerator Center, Stanford University, Nov. 1984).
- [15] HASTIE, T. and STUETZLE, W., ‘Principal Curves’, *J. Amer. Statist. Assoc.* 84/406 (1989), 502–16. doi: 10 . 2307 / 2289936.

-
- [16] HINRICHS, A., NOVAK, E., and WOŹNIAKOWSKI, H., ‘The curse of dimensionality for the class of monotone functions and for the class of convex functions’, *J. Approx. Theory*, 163/8 (2011), 955–65. doi: 10.1016/j.jat.2011.02.009.
 - [17] HU, S.-M. and WALLNER, J., ‘A second order algorithm for orthogonal projection onto curves and surfaces’, *Comput. Aided Geom. Design*, 22/3 (2005), 251–60. doi: 10.1016/j.cagd.2004.12.001.
 - [18] ISMAILOV, V. E., ‘Approximation by ridge functions and neural networks with a bounded number of neurons’, *Appl. Anal.* 94/11 (2015), 2245–60. doi: 10.1080/00036811.2014.979809.
 - [19] JOHN, F., *Plane Waves and Spherical Means Applied to Partial Differential Equations*, Reprint of the 1955 original (New York: Springer-Verlag, 1981).
 - [20] JORGENSEN, P. and STEWART, D. E., ‘Approximation properties of ridge functions and extreme learning machines’, *SIAM J. Math. Data Sci.* 3 (2021). doi: 10.1137/20M1356348.
 - [21] KEIPER, S., ‘Approximation of generalized ridge functions in high dimensions’, *J. Approx. Theory*, 245 (2019), 101–29. doi: 10.1016/j.jat.2019.04.006.
 - [22] KOLLECK, A. and VYBIRAL, J., ‘On some aspects of approximation of ridge functions’, *J. Approx. Theory*, 194 (2015), 35–61. doi: 10.1016/j.jat.2015.01.003.
 - [23] KONOVALOV, V. N., KOPOTUN, K. A., and MAIOROV, V. E., ‘Convex polynomial and ridge approximation of Lipschitz functions in \mathbb{R}^d ’, *Rocky Mountain J. Math.* 40/3 (2010), 957–76. doi: 10.1216/RMJ-2010-40-3-957.
 - [24] KROÓ, A., ‘On approximation by ridge functions’, *Constr. Approx.* 13/4 (1997), 447–60. doi: 10.1007/s003659900053.
 - [25] LIANG, J. et al., ‘Hybrid second order method for orthogonal projection onto parametric curve in n-dimensional Euclidean space’, *Mathematics*, 6/12 (2018). doi: 10.3390/math6120306.
 - [26] LIMAIEM, A. and TROCHU, F., ‘Geometric algorithms for the intersection of curves and surfaces’, *Comput. & Graphics*, 19/3 (1995), 391–403. doi: 10.1016/0097-8493(95)00009-2.
 - [27] LIN, V. Y. and PINKUS, A., ‘Fundamentality of ridge functions’, *J. Approx. Theory*, 75/3 (1993), 295–311. doi: 10.1006/jath.1993.1104.
 - [28] LOGAN, B. F. and SHEPP, L. A., ‘Optimal reconstruction of a function from its projections’, *Duke Math. J.* 42/4 (1975), 645–59. doi: 10.1215/S0012-7094-75-04256-8.
 - [29] MAIOROV, V. E., ‘On best approximation by ridge functions’, *J. Approx. Theory*, 99/1 (1999), 68–94. doi: 10.1006/jath.1998.3304.
 - [30] MAIOROV, V., ‘Geometric properties of the ridge function manifold’, *Adv. Comput. Math.* 32/2 (2010), 239–53. doi: 10.1007/s10444-008-9106-3.
 - [31] MAYER, S., ULLRICH, T., and VYBIRAL, J., ‘Entropy and sampling numbers of classes of ridge functions’, *Constr. Approx.* 42/2 (2015), 231–64. doi: 10.1007/s00365-014-9267-x.
 - [32] MOLLWEIDE, K. B., ‘Zusätze zur ebenen und sphärischen Trigonometrie’, *Mon. Corresp. Befoerd. Erd Himmelskunde*, 18 (Nov. 1808), 394–400.
 - [33] NOVAK, E. and WOŹNIAKOWSKI, H., ‘Approximation of infinitely differentiable multivariate functions is intractable’, *J. Complexity*, 25/4 (2009), 398–404. doi: 10.1016/j.jco.2008.11.002.
 - [34] PETRUSHEV, P. P., ‘Approximation by ridge functions and neural networks’, *SIAM J. Math. Anal.* 30/1 (1999), 155–89. doi: 10.1137/S0036141097322959.
 - [35] PINKUS, A., ‘Approximation theory of the MLP model in neural networks’, *Acta Numer.* 8 (1999), 143–95. doi: 10.1017/S0962492900002919.
-

-
- [36] ROCKAFELLAR, R. and WETS, R. J.-B., *Variational Analysis* (Grundlehren der mathematischen Wissenschaften. A Series of Comprehensive Studies in Mathematics, 317; Dortrecht: Springer, 2009). doi: 10 . 1007 / 978 - 3 - 642 - 02431 - 3.
 - [37] SARD, A., 'The measure of the critical values of differentiable maps', *Bull. Amer. Math. Soc.* 48/12 (1942), 883–90. doi: 10 . 1090 / S0002 - 9904 - 1942 - 07811 - 6.
 - [38] SONG, H.-C. et al., 'Projecting points onto planar parametric curves by local biarc approximation', *Comput. & Graphics*, 38 (2014), 183–90. doi: 10 . 1016 / j . cag . 2013 . 10 . 033.
 - [39] TYAGI, H. and CEVHER, V., 'Learning ridge functions with randomized sampling in high dimensions', in *Proceedings of the ICASSP (25-30 March 2012, Kyoto, Japan)*, IEEE (2012), 2025–8. doi: 10 . 1109 / ICASSP . 2012 . 6288306.
 - [40] XIE, T. F. and CAO, F. L., 'The ridge function representation of polynomials and an application to neural networks', *Acta Math. Sin. (Engl. Ser.)*, 27/11 (2011), 2169–76. doi: 10 . 1007 / s10114 - 011 - 9407 - 1.
-